Available online at www.sciencedirect.com
ScienceDirect
Ceramics International 37 (2011) 3389–3395
CERAMICS INTERNATIONAL
www.elsevier.com/locate/ceramint

Mössbauer spectroscopic and chromaticity analysis on colorative mechanism of celadon glaze

Jong-Young Kim [a,*], Hyunggoo No [a], A. Young Jeon [a], Ungsoo Kim [a], Jae-Hwan Pee [a], Woo-Seok Cho [a], Kyung Ja Kim [a], Chin Mo Kim [b], Chul Sung Kim [b]

[a] *Icheon Branch, Korea Institute of Ceramic Engineering and Technology, Gyeongchung Rd., Sindun-Myeon, Icheon-si, Kyeonggi-do 467-843, Republic of Korea*
[b] *Department of Physics, Kookmin University, Seoul 136-702, Republic of Korea*

Received 25 May 2011; received in revised form 30 May 2011; accepted 30 May 2011
Available online 15 June 2011

Abstract

The dependence of the color of a celadon glaze on the chemical composition and the electronic state of Fe was investigated by Mössbauer spectroscopic and chromaticity analysis. The amount of Fe_2O_3 was found to be the main factor influencing L^* and b* values, whereas the amount of TiO_2 was found to affect all the parameters (L^*, a^*, b^*). The effect of MnO on the color was significant only by interaction terms. The amount of P_2O_5 was found to be the main factor of the b^* value. According to the Mössbauer analysis results, as the amount of divalent iron ions increases, the a^* and b^* values decreased; on the other hand, the L^* value increased. As the amount of titanium increased, Fe^{2+} was found to be destabilized relative to Fe^{3+} due to the structural instability of Fe–O–Ti network.

Keywords: Celadon; Mössbauer; Color; Glaze

1. Introduction

The color of a celadon is developed through the formation of glassy and crystalline phases, which are generated by chemical reactions between the glaze and the clay-based body during the firing process at high temperature [1,2]. The glaze is generally composed of feldspar, lime stone, and clay minerals. Feldspar is used as a flux material to form the glassy phase, and a small amount of Fe acts as a color former in the glassy phase. Therefore, the color and glossiness of the celadon are significantly influenced by the Fe ions. The coloration of the celadon is known to depend on the amount of ferrous oxide (FeO) present in the glaze and on the ionic states (Fe^{2+}, Fe^{3+}) of iron oxide [3–7]. However, it is very difficult to measure change in the electronic state of Fe in celadon because a very small amount of iron (<3%) exists in a non-crystalline amorphous form. In this respect, Mössbauer spectroscopy is a very useful technique to investigate the ionic states of iron in celadon glaze because it allows us to analyze samples containing very small amounts of Fe [8,9]. In the present work, we attempted to shows how the electronic state of Fe is related to the coloration of celadon glaze by Mössbauer spectroscopy.

Furthermore, the relationship between the chemical composition of the coloring elements such as Fe_2O_3, TiO_2, MnO, P_2O_5 and the chromaticity were systematically investigated by a statistical method of DOE (Design of Experiment) analysis. Because several coloring elements are involved in the celadon glaze, we attempted to elucidate the main effects and interactions of the chemical elements on the coloration quantitatively by DOE analysis. The range of the coloring elements was selected in the values obtained from the ancient celadon from Gangjin, a small town in the southern part of Korea, known for Goryeo celadon since the Goryeo Dynasty (A.D. 918–1392).

For the present work, the values of L^*, a^*, and b^* in CIE (Commission internationale de l'éclairage) space were measured and their relation to the chemical composition was determined by a DOE (Design of Experiment) analysis. Furthermore, the relationship between the electronic state of Fe and the chromaticity of the celadon glaze was investigated by Mössbauer spectroscopy. Through the combined results, the relationship between the coloration of the celadon glaze and the

* Corresponding author. Tel.: +82 31 645 1423; fax: +82 31 645 1486.
E-mail address: jykim@kicet.re.kr (J.-Y. Kim).

0272-8842/$36.00
doi:10.1016/j.ceramint.2011.05.141

Table 1
Chemical composition of a basic glaze.

Component	SiO_2	Al_2O_3	Na_2O	K_2O	MgO	CaO	Fe_2O_3	TiO_2	P_2O_5
wt%	67.42	14.28	0.23	2.50	0.41	14.97	0.11	0.03	0.05

chemical states of the coloring elements was quantitatively evaluated.

2. Experimental

The chemical composition of a basic glaze and the sintering conditions are listed in Tables 1 and 2. The chemical compositions of the coloring oxides of Fe_2O_3, TiO_2, MnO, and P_2O_5 are listed in Table 3 with the measured L^*, a^*, and b^* values. In this work, a whiteware background was used to minimize the effect of Fe in the background on the chromaticity of the glaze. The basic glaze and the coloring elements were mixed in a pot mill for 24 h with a dispersant (1% cerasperse). The glaze was sprayed on the whiteware background (50 mm × 50 mm), calcined at 900 °C, and then sintered at 1260 °C in a reducing atmosphere (Fig. 1). When the temperature reached 900 °C, a mixed gas comprising air and LPG was used to induce a reducing atmosphere. The gas flowing condition was controlled as shown in Table 2.

The optical spectra for the sintered specimens were measured by a Cary 100 UV-Visible Spectrophotometer and the L^*, a^*, b^* values of the specimens were obtained in CIE space (Fig. 2). The DOE analysis was performed by MINITAB software. The Mössbauer spectra were recorded with a fixed absorber and a moving source by using a conventional electromechanical type spectrometer. A ^{57}Co source in a Rh matrix manufactured by Dupont was used at room temperature. To produce a uniform thickness over the area of the Mössbauer absorber, the amount of each sample was adjusted for ^{57}Fe density of 0.214 mg/cm^2 and the sample was clamped between two beryllium disks with thickness of 0.005 in. and diameter of 1 in.

3. Results and discussion

3.1. The chromaticity and the chemical composition

Typical colors dependent on the addition of Fe_2O_3, TiO_2, MnO, and P_2O_5 was shown in Fig. 3, and the measured L^*, a^*, b^* values are listed in Table 3. The L^* values range from N8.7 to N4.6 according to the composition, and the color is mainly BG (Blue–Green) and GY (Green–Yellow), respectively. When the addition of TiO_2 is 0.1%, the color of the present system is found to be BG, and when the addition is 1.0%, the color is found to be GY. For the GY group, the colors change from GY to YR (Yellow–Red) with a decrease of brightness upon increased addition of TiO_2, MnO, and P_2O_5.

We attempted to analyze the effect of the chemical composition on the L^*, a^*, b^* values by a DOE (Design of Experiment) analysis. The experimental matrix for the DOE was designed as presented in Table 3, and the terms affecting the L^*, a^*, and b^* values, including the main effect and 2nd/3rd order interaction effects, were obtained. In the DOE, when a P-value of a term is smaller than 0.05, the term is regarded as statistically significant within a confidence level of 95%. Larger T value and coefficient of a term in Table 4 indicate more significant influence on the chromaticity (L^*, a^*, b^*). A larger gradient of a term in the main effect plot (upper plot of Fig. 4) and a larger difference between gradients of terms in the

Table 2
Conditions of reductive sintering.

Gas	Air (ℓ/min)	LPG (ℓ/min)	O_2 (%)
Flow rate	5.0	0.7	18.42

Table 3
L^*, a^*, and b^* values according to coloring oxide composition.

Sample no.	Composition				chromaticity		
	Fe_2O_3	TiO_2	MnO	P_2O_5	L^*	a^*	b^*
1	1.40	0.10	0.20	1.30	78.88	−7.77	6.53
2	1.40	1.0	0.80	0.30	71.92	−1.74	25.21
3	1.40	1.0	0.20	1.30	69.77	−0.34	28.51
4	2.20	0.10	0.20	1.30	76.03	−7.67	6.26
5	1.40	1.0	0.20	0.30	69.45	−1.59	26.15
6	2.20	1.0	0.20	1.30	62.61	1.90	29.97
7	2.20	0.10	0.80	1.30	72.37	−7.46	9.41
8	2.20	1.0	0.20	0.30	67.96	−1.43	26.43
9	0	0	0	0	87.15	−1.59	0.19
10	1.40	1.0	0.20	1.30	68.83	−0.01	28.26
11	1.40	0.10	0.20	0.30	79.69	−6.98	4.08
12	1.40	1.0	0.80	1.30	72.28	−1.47	25.92
13	2.20	0.10	0.20	0.30	76.44	−8.68	4.58
14	2.20	0.10	0.20	0.30	74.49	−8.40	6.93
15	2.20	1.0	0.80	1.30	64.96	0.21	28.91
16	1.40	0.10	0.80	1.30	79.78	−6.79	4.64
17	1.40	0.10	0.80	1.30	78.43	−7.73	6.29
18	2.20	0.10	0.20	1.30	71.19	−7.85	9.05
19	1.40	1.0	0.80	1.30	69.35	0.05	28.77
20	1.40	0.10	0.20	1.30	78.68	−7.41	6.82
21	2.20	0.10	0.80	1.30	76.74	−7.69	6.33
22	2.20	0.10	0.80	0.30	74.72	−7.22	7.87
23	2.20	1.0	0.20	1.30	61.20	2.31	30.00
24	1.40	0.10	0.80	0.30	79.17	−6.71	5.10
25	2.20	1.0	0.80	0.30	63.71	0.65	28.65
26	0	0	0	0	81.90	−0.89	2.04
27	1.40	0.10	0.80	0.30	79.23	−6.39	4.87
28	1.40	1.0	0.20	0.30	69.66	−1.80	25.40
29	2.20	1.0	0.80	0.30	53.54	10.44	31.42
30	1.40	1.0	0.80	0.30	74.11	−1.30	23.31
31	0	0	0	0	86.95	−1.54	0.76
32	2.20	0.10	0.80	0.30	76.84	−8.30	4.93
33	2.20	1.0	0.80	1.30	62.94	1.63	30.09
34	1.40	0.10	0.20	0.30	79.06	−7.08	4.32
35	2.20	1.0	0.20	0.30	67.68	−1.54	26.99

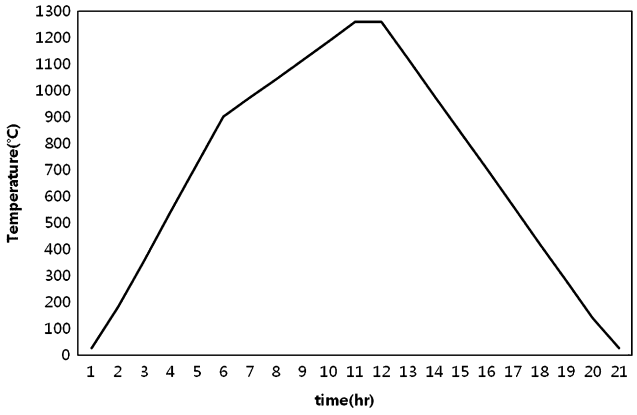

Fig. 1. Sintering schedule.

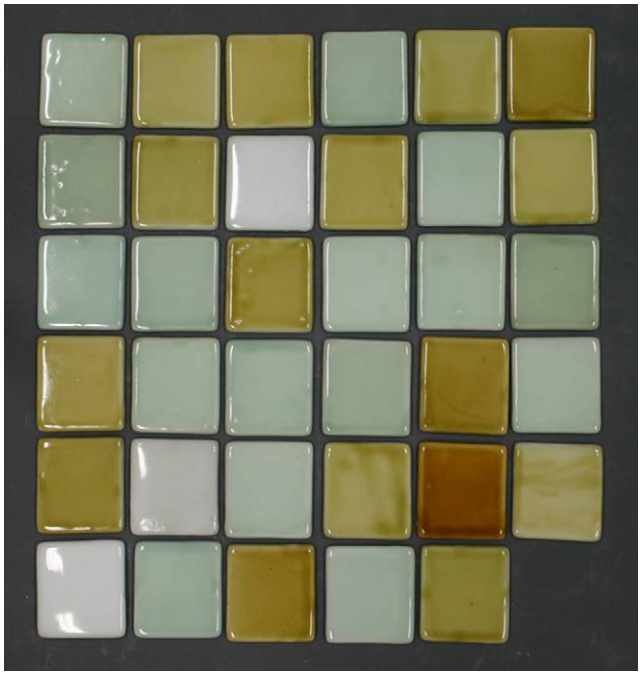

Fig. 3. Typical celadon tiles after sintering.

interaction plot (lower plot of Fig. 4) means more interaction effect between the terms on the chromaticity [10].

The range of the amounts of Fe_2O_3, TiO_2, MnO, and P_2O_5 was selected according to values obtained from the Goryeo celadon from Gangjin. Accordingly, the level of solid content was fixed at 1.4/2.2% for Fe_2O_3, 0.1/1.0% for TiO_2, 0.2/0.8% for MnO, 0.3/1.3% for P_2O_5, respectively.

As for the brightness, the terms of Fe_2O_3 and TiO_2 are found to be significant in relation to the L^* value, which is indicated by their large gradients in Fig. 4(a). The effects of Fe_2O_3 and TiO_2 are larger than those of MnO and P_2O_5, which is indicated by lower P-values as shown in Table 4a. The interactions of $Fe_2O_3 \times TiO_2$ and $Fe_2O_3 \times TiO_2 \times MnO$ are relatively significant as shown by low P-values (0.06, 0.09).

As for the a^* value, TiO_2, $Fe_2O_3 \times TiO_2$, $MnO \times P_2O_2$, and $TiO_2 \times MnO \times P_2O_5$ are found to be significant, as shown by

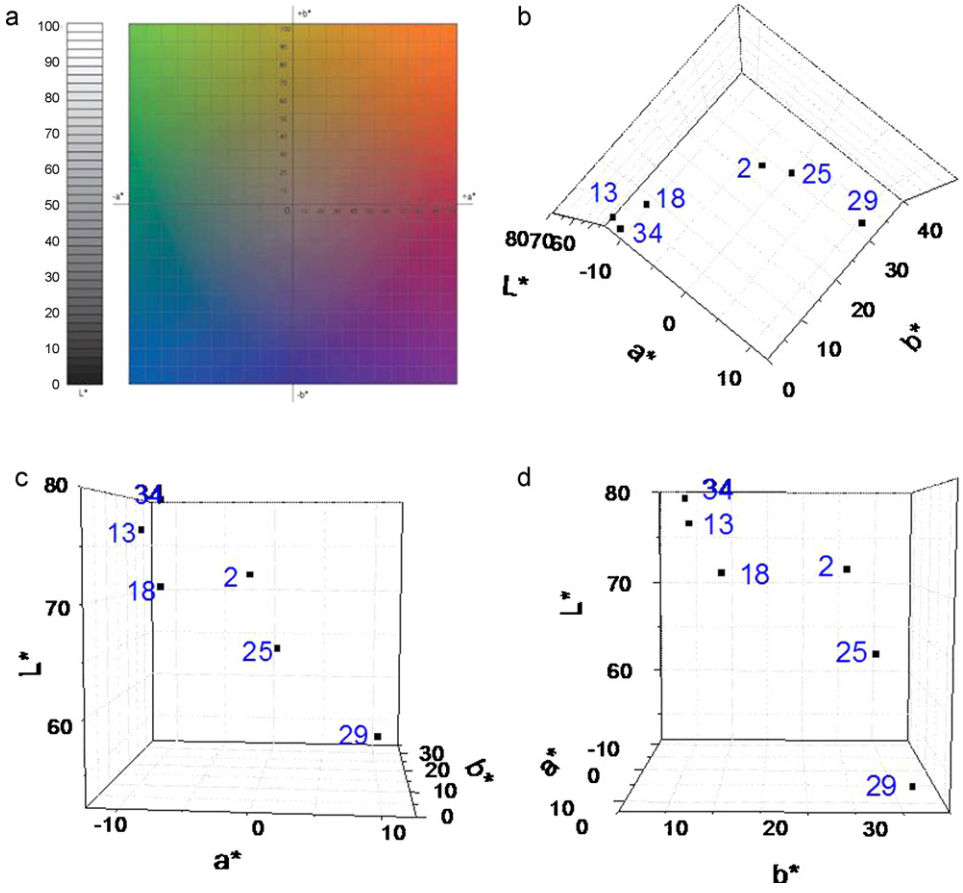

Fig. 2. (a) CIE space, (b) L^*, (c) a^*, and (d) b^* values for the samples measured by Mössbauer spectroscopy.

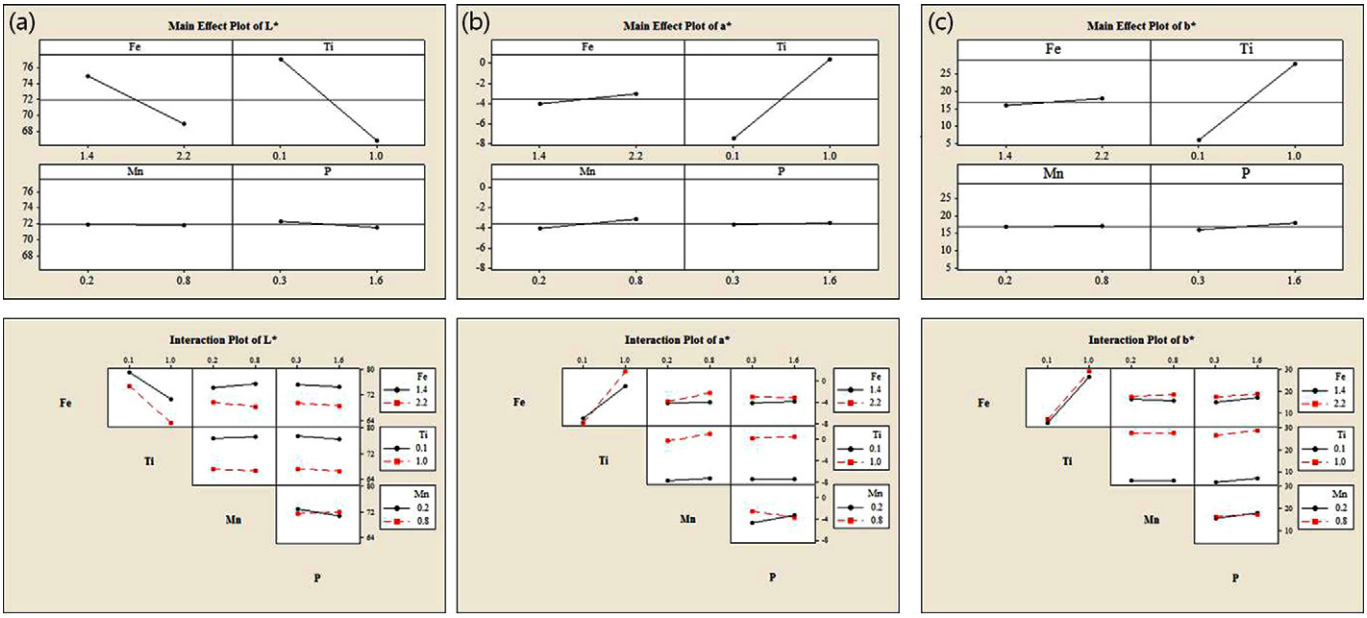

Fig. 4. Terms of main effect/interaction effect on (a) L^*, (b) a^*, and (c) b^* values.

the P-values. As the a^* value is mainly dominated by TiO_2 and the interaction terms with TiO_2, as shown by the low P-values in Table 4b. However, Fe_2O_3 does not have a significant main effect on the a^* value and is only significant through interaction with TiO_2.

As shown in Table 4c, the terms of Fe_2O_3, TiO_2, P_2O_5, $Fe_2O_3 \times TiO_2$, and $MnO \times P_2O_5$ are found to be significant for the b^* value. As the effect of P_2O_5 is significant for the b^* value, as the amounts of P_2O_5 increased, the color becomes GY (Green–Yellow) and YR (Yellow–Red).

In summary, the amount of Fe_2O_3 was found to be a main factor of the L^* and b^* values in the present system and the amount of TiO_2 was found to be a main factor for all the parameters (L^*, a^*, b^*) in the present system. The effect of MnO on the color is not significant independently and is significant only by interaction terms. The amount of P_2O_5 was found to be a main factor of the b^* value, and an increase of P_2O_5 leads to a change from BG to GY.

3.2. Mössbauer analysis

As shown in Table 5, Mössbauer spectra at room temperature were analyzed by two components with a doublet and a single line shape, which can be attributed to Fe^{2+} and Fe^{3+}, respectively. No samples exhibited magnetic behaviors at room temperature. The value of δ represents the isomer shift of Fe ions, and the area indicates the relative area ratio of Fe^{2+} and Fe^{3+}, and ΔE_Q is the strength of the electric quadrupole interaction (electric quadrupole splitting).

As shown in Table 5, as the ratio of Fe^{2+} to Fe^{3+} increases, the a^* and b^* values decrease. As shown in Figs. 5 and 6, as the ratio of Fe^{2+} to Fe^{3+} increases, the peak position in the UV-

Table 4a
DOE results for the L^* values.

Terms	Effect	Coeff.	T	P
Constant		71.9284	177.73	0
Block		0.5553	1.37	0.19
Fe_2O_3	−5.929	2.9647	7.33	0
TiO_2	−10.111	5.0553	12.49	0
MnO	−0.096	0.0478	0.12	0.908
P_2O_5	−0.852	0.4259	1.05	0.309
$Fe_2O_3 \times TiO_2$	−1.667	−0.8334	−2.06	0.057
$Fe_2O_3 \times MnO$	−1.377	−0.6884	−1.7	0.11
$Fe_2O_3 \times P_2O_5$	−0.066	−0.0328	−0.08	0.936
$TiO_2 \times MnO$	−0.448	−0.2241	−0.55	0.588
$TiO_2 \times P_2O_5$	0.091	0.0453	0.11	0.912
$MnO \times P_2O_5$	1.303	0.6516	1.61	0.128
$Fe_2O_3 \times TiO_2 \times MnO$	−1.654	0.8272	2.04	0.059
$Fe_2O_3 \times TiO_2 \times P_2O_5$	0.532	−0.2659	−0.66	0.521
$Fe_2O_3 \times MnO \times P_2O_5$	1.664	−0.8322	−2.06	0.058
$TiO_2 \times MnO \times P_2O_5$	1.021	−0.5103	−1.26	0.227
$Fe_2O_3 \times TiO_2 \times MnO \times P_2O_5$	1.632	0.8159	2.02	0.062

Table 4b
DOE results for the a^* values.

Terms	Effect	Coeff.	T	P
Constant		−3.5675	−11.39	0
Block		−0.3756	−1.2	0.249
Fe_2O_3	0.998	−0.4988	−1.59	0.132
TiO_2	7.881	−3.9406	−12.58	0
MnO	0.907	−0.4537	−1.45	0.168
P_2O_5	0.124	−0.0619	−0.2	0.846
$Fe_2O_3 \times TiO_2$	1.799	0.8994	2.87	0.012
$Fe_2O_3 \times MnO$	0.795	0.3975	1.27	0.224
$Fe_2O_3 \times P_2O_5$	−0.141	−0.0706	−0.23	0.825
$TiO_2 \times MnO$	0.464	0.2319	0.74	0.47
$TiO_2 \times P_2O_5$	0.2	0.1	0.32	0.754
$MnO \times P_2O_5$	−1.209	−0.6044	−1.93	0.073
$Fe_2O_3 \times TiO_2 \times MnO$	0.756	−0.3781	−1.21	0.246
$Fe_2O_3 \times TiO_2 \times P_2O_5$	−0.7	0.35	1.12	0.281
$Fe_2O_3 \times MnO \times P_2O_5$	−0.994	0.4969	1.59	0.133
$TiO_2 \times MnO \times P_2O_5$	−1.023	0.5113	1.63	0.123
$Fe_2O_3 \times TiO_2 \times MnO \times P_2O_5$	−0.883	−0.4413	−1.41	0.179

Table 4c
DOE results for the b^* values.

Terms	Effect	Coeff.	T	P
Constant		16.9375	71.31	0
Block		−0.1738	−0.73	0.476
Fe_2O_3	2.1025	−1.0513	−4.43	0
TiO_2	21.6238	−10.8119	−45.52	0
MnO	0.09	−0.045	−0.19	0.852
P_2O_5	1.845	−0.9225	−3.88	0.001
$Fe_2O_3 \times TiO_2$	0.5138	0.2569	1.08	0.297
$Fe_2O_3 \times MnO$	0.835	0.4175	1.76	0.099
$Fe_2O_3 \times P_2O_5$	−0.3175	−0.1588	−0.67	0.514
$TiO_2 \times MnO$	−0.0187	−0.0094	−0.04	0.969
$TiO_2 \times P_2O_5$	0.2638	0.1319	0.56	0.587
$MnO \times P_2O_5$	−0.72	−0.36	−1.52	0.15
$Fe_2O_3 \times TiO_2 \times MnO$	0.5138	−0.2569	−1.08	0.297
$Fe_2O_3 \times TiO_2 \times P_2O_5$	−0.4213	0.2106	0.89	0.389
$Fe_2O_3 \times MnO \times P_2O_5$	−0.34	0.17	0.72	0.485
$TiO_2 \times MnO \times P_2O_5$	−0.1138	0.0569	0.24	0.814
$Fe_2O_3 \times TiO_2 \times MnO \times P_2O_5$	−0.7313	−0.3656	−1.54	0.145

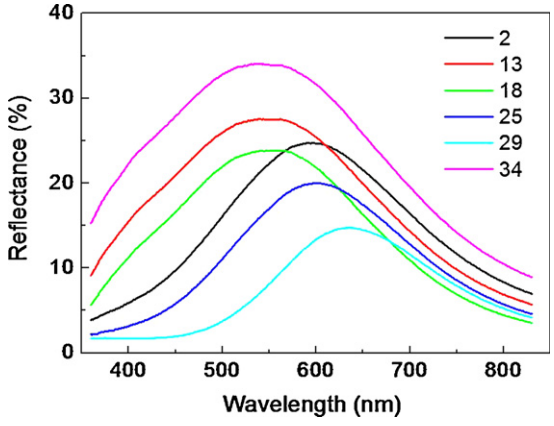

Fig. 5. UV reflectance spectra for celadon samples.

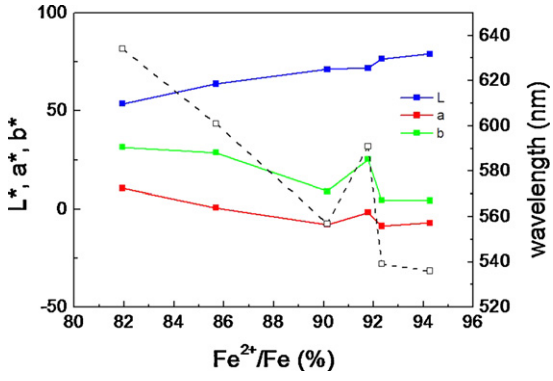

Fig. 6. Evolution of L^*, a^*, b^* values and wavelength at max reflectance in UV spectra according to $Fe^{2+}/(Fe^{3+} + Fe^{3+})$ ratio.

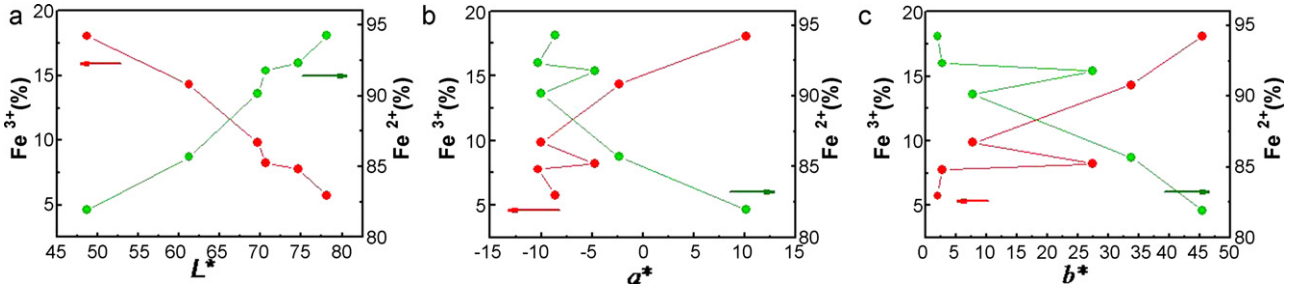

Fig. 7. Evolution of (a) L^*, (b) a^*, and (c) b^* values according to Fe^{2+}, Fe^{3+} area.

reflectance spectrum shifts toward low wavelength (high energy). This is consistent with the coloring turning into BG as the a^* and b^* values decrease. Besides, the a^* and b^* values, as the ratio of Fe^{2+} to Fe^{3+} increases, the L^* value (brightness) increases (Fig. 7).

Furthermore, the ratios of Fe^{2+} to Fe^{3+} is found to be related to the amount of TiO_2 in the glaze (Fig. 8). When the amount of Ti is 1.0 wt% (**2**, **25**, and **29**), the ratios of Fe^{2+} to Fe^{3+} is 82–92%, which is smaller than 90–94% when the amount of TiO_2 is 0.1 wt% (**34**, **13**, **18**). This is probably related to the effect of Ti^{4+} on the stability of Fe^{3+} relative to Fe^{2+} in the glaze. The previous work on a redox equilibria of Fe in Ti-bearing glass showed that Ti^{4+} in silicate glasses tends to enhance the stability of Fe^{3+} relative to that of Fe^{2+} due to the structural instability of Fe^{2+}–O–Ti^{4+} network [11]. Because of the considerably larger size of Ti^{4+} than Si^{4+}, the ferrous oxygen polyhedra might be

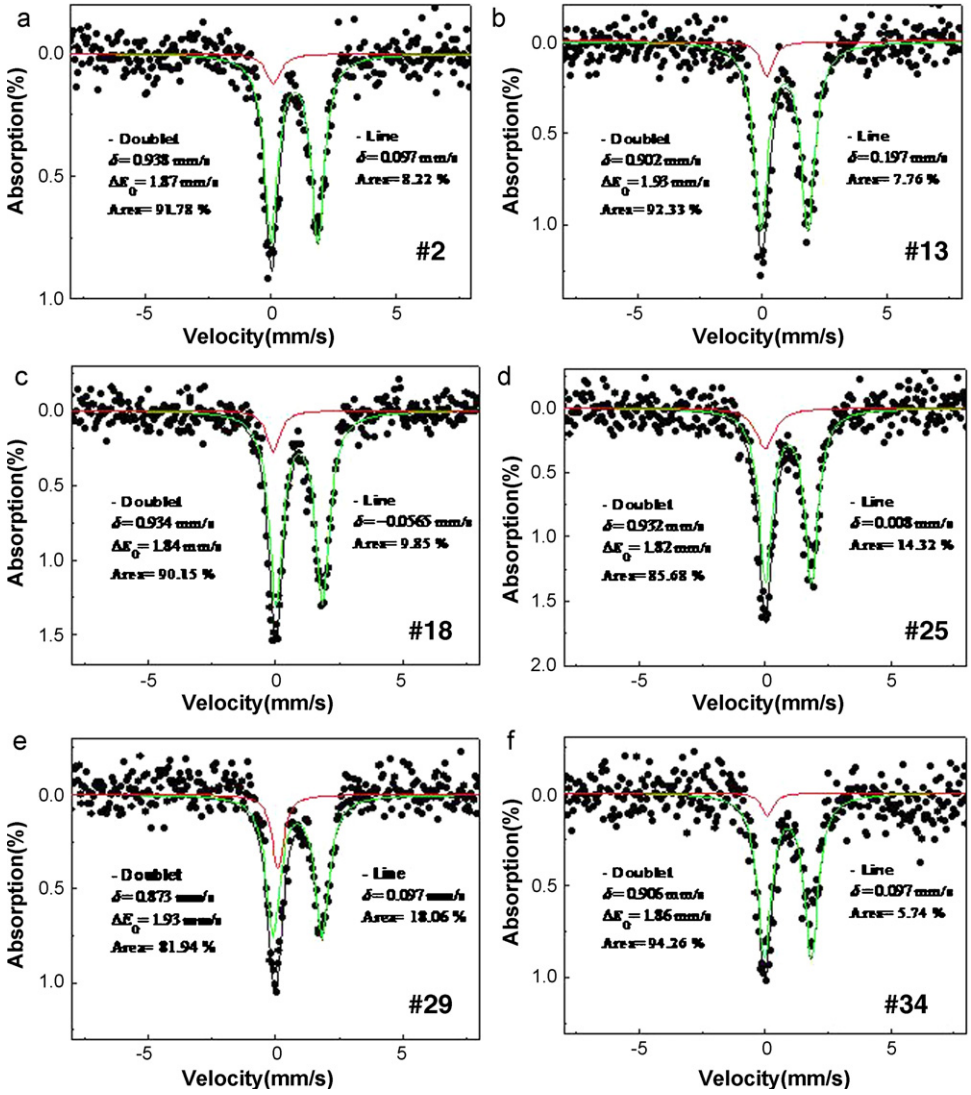

Fig. 8. Mössbauer spectra at room temperature for the samples of (a) 2, (b) 13, (c) 18, (d) 25, (e) 29, and (f) 34.

Table 5
Mössbauer analysis results.

Sample	L^*	a^*	b^*	Fe^{3+} *1line* (*red line*)		Fe^{2+} *Doublet 1* (*green line*)		
				δ (mm/s)	Area (%)	ΔE_Q (mm/s)	δ (mm/s)	Area (%)
34	79.06	−7.08	4.32	0.0965	5.74	1.8593	0.9056	94.26
13	76.44	−8.68	4.58	0.1972	7.76	1.9253	0.9015	92.33
2	71.92	−1.74	25.21	0.0968	8.22	1.8651	0.9383	91.78
18	71.19	−7.85	9.05	−0.0565	9.85	1.8387	0.9343	90.15
25	63.71	0.65	28.65	0.0081	14.32	1.8151	0.9323	85.68
29	53.54	10.44	31.42	0.0965	18.06	1.9253	0.8726	81.94

more distorted when linked to tetrahedral titanium rather than to silicon. Therefore, the distortion of Fe^{2+}–O polyhedra leads to the destabilization and subsequent oxidation of the ferrous iron.

4. Conclusion

The composition of Fe_2O_3, TiO_2, MnO, and P_2O_5 in a celadon glaze was controlled in the range of ancient celadon from Gangjin, and the relationship between the coloring oxides and the chromaticity was quantitatively analyzed by a chromaticity analysis and Mössbauer spectroscopy. The effects of the composition on the L^*, a^*, and b^* values were systematically analyzed by a DOE analysis. The brightness (L^*) is mainly affected by the amount of Fe_2O_3 and TiO_2, whereas the effects of MnO and P_2O_5 were negligible. The a^* value is mainly affected by the amount of TiO_2 and its interactions with Fe_2O_3 and MnO/P_2O_5. The b^* value is affected by the amounts of Fe_2O_3, TiO_2, and P_2O_5, and the interaction between MnO and P_2O_5. According to the Mössbauer spectroscopic results, as the ratio of Fe^{2+} to Fe^{3+} increases, the a^* and b^* values decreases; on the other hand, the L^* value increases. The peak position in the UV-reflectance spectrum is found to shift toward the low wavelength (high energy) side. The ratio of Fe^{2+} to Fe^{3+} ranges from 80% to 95%, which results in an increase of the brightness.

Acknowledgement

This work was supported by a grant from the Ministry of Knowledge Economy.

References

[1] C.K. Koh-Choo, Y.E. Lee, I.W. Shim, G.H. Kim, W.Y. Huh, S.C. Chun, W.K. Choo, Compositional and microstructural study of Koryo celadon and whiteware excavated from Sori kiln in Kyonggi province, Archaeometry 46 (2004) 247–265.
[2] F. William, M. Devitt, Effect of firing atmosphere on development of colors in ceramic glazes, J. Am. Ceram. Soc. 27 (1944) 165–175.
[3] B. Zhang, Z. Gao, W. Zhao, G. Li, H. Cheng, Z. Zhang, Mössbauer spectroscopy and neutron activation analysis of ancient Chinese glazes, Appl. Clay Sci. 25 (2004) 161–165.
[4] B. Zhang, Y.L. Liu, Z.Y. Gao, W.J. Zhao, G.X. Liand, H.S. Cheng, Mössbauer spectroscopy, NAA and PIXE study on some archeological problems of ancient Chinese Ru celadon, Hyperfine Interact. 163 (2005) 1–12.
[5] Y. Yang, M. Feng, X. Ling, Z. Mao, C. Wang, X. Sun, M. Guo, Microstructural analysis of the color-generating mechanism in Ru ware, modern copies and its differentiation with Jun ware, J. Archaeolog. Sci. 32 (2005) 301–310.
[6] G. Zhengyao, C. Songhua, C. Xiande, Mössbauer study of the Ru porcelain of Chinese Song Dynasty and Yuan Dynasty, Hyperfine Interact. 91 (1994) 663–668.
[7] Z. Bin, G. Zhengyao, NAA and Mössbauer study on the colorative mechanism of Yaozhou celadon in ancient China, Hyperfine Interact. 142 (2002) 593–599.
[8] W. Kim, C.H. Rhee, H.J. Kim, S.J. Moon, C.S. Kim, Strong crystalline field at the Fe site and spin rotation in olivine $LiNi_{0.99}{}^{57}Fe_{0.01}PO_4$ material by Mössbauer spectroscopy, Appl. Phys. Lett. 96 (2010) 242505–242507.
[9] I.K. Lee, I.B. Shim, C.S. Kim, Temperature dependent valence states and magnetic properties of lithium delithiated $Li_{0.59}FePO_4$, J. Appl. Phys. 107 (2010) 09A522–19A.
[10] Minitab Inc., Designing an experiment, Meet Minitab 15, 2007 (Chapter 5).
[11] H.V. Alberto, J.M. Gil, N. Ayres DeCampos, B.O. Mysen Redox, Equilibria of iron in Ti-bearing calcium silicate quenched glasses, J. Non-Cryst. Solids 151 (1992) 39–50.